RESULTS AND LESSONS LEARNED FROM THE FIRST FIELD TRIAL OF THE ESA-ESRIC SPACE RESOURCES CHALLENGE OF TEAM GLIMPSE

Philip Arm[1], Gabriel Waibel[1], Gabriela Ligeza[2], Valentin Bickel[3], Marco Tranzatto[1], Samuel Zimmermann[1], Timon Homberger[1], Lars Horvath[4], Hugo Umbers[4], Florian Kehl[5,6,7], Hendrik Kolvenbach[1], and Marco Hutter[1]

[1]*Robotic Systems Lab, ETH Zurich, Leonhardstr. 21, 8092 Zurich, Switzerland*
[2]*Department of Environmental Sciences, University of Basel, 4056 Basel, Switzerland*
[3]*Engineering Geology, ETH Zurich, Sonneggstr. 5, 8092 Zurich, Switzerland*
[4]*Department of Information Technology and Electrical Engineering, ETH Zurich*
[5]*Innovation Cluster Space and Aviation (UZH Space Hub), Air Force Center, University of Zurich, 8600 Dübendorf, Switzerland*
[6]*Institute of Anatomy, Faculty of Medicine, University of Zurich, 8057 Zurich, Switzerland*
[7]*Institute of Medical Engineering, Space Biology Group, Lucerne University of Applied Sciences and Arts, 6052, Hergiswil, Switzerland*

ABSTRACT

Resource prospection is a crucial step toward off-world in-situ resource utilization, sustainable exploration, and long-term habitation. The European Space Agency and the European Space Resources Innovation Centre initiated the Space Resources Challenge to assess current European and Canadian off-world resource prospection technologies and accelerate the development of key technologies. We present GLIMPSE, the Geological Lunar In-Situ Mapper and Prospector for Surface Exploration, which is our contribution to this challenge. GLIMPSE builds upon the legged robot ANYmal. We successfully use state-of-the-art locomotion, navigation and mapping systems, and scientific payloads to prospect samples during the first field trial of the Space Resources Challenge. We conclude this work with lessons learned and a list of identified requirements for future robotic prospection technologies.

Key words: Field Test, Resource Prospection, Legged Robots, Planetary Robotics.

1. INTRODUCTION

As exploration evolves toward longer and sustainable journeys far away from earth, in-situ resource utilization (ISRU) is becoming increasingly important. However, before resources can be extracted and processed, they need to be identified, characterized, and contextualized. Thorough prospection of resources and their environment is vital in identifying the most promising sites for extraction and - more importantly - permanent and sustainable habitation. Therefore, many private and public entities in the space industry prioritize prospecting activities in their technology development and mission portfolios. The European Space Agency (ESA) states that establishing volatiles at the lunar poles and regolith and pyroclastic deposits across the lunar surface is a core priority in the ESA Space Resources Strategy [1]. NASA mentions robotic prospecting as essential for human habitation [2] and plans the launch of the Volatiles Investigating Polar Exploration Rover (VIPER) in 2023. The rover's mission is to investigate volatiles at the lunar south pole [3]. It is important to note that some of the most relevant resources on the Moon, including water-ice and sunlight, are most abundant in environmentally challenging regions, such as the south pole [4]. Challenges involve i.a., rough, steep, and granular terrain, disadvantageous illumination conditions, and high-latency Direct-To-Earth communication. Before robotic prospection missions can commence in such areas, technological advancements in robotic mobility, mapping, autonomy, payload development, and science operation capabilities are required.

Figure 1: We equipped ANYmal with state-of-the-art sensors for navigation, mapping and localization, and a broad scientific instrument suite for resource prospection.

In this context, ESA and the European Space Resources Innovation Centre (ESRIC) started the Space Resources Challenge (SRC) to evaluate and advance lunar robotic prospecting technologies. The challenge contains two phases, each concluded by an evaluated field deployment. The first deployment took place in November 2021 in a lunar analog environment in the Netherlands, simulating the adverse conditions at the lunar south pole: a priori unknown terrain, including unconsolidated, granular soil and steep slopes, high solar incidence angle illumination, and network communications with high latency ($5\,\mathrm{s}$ round trip time) and intermittent complete loss of signal. The goal during this trial was to navigate through a traversal zone to a distinct Region of Interest (ROI), identify rock samples scattered across the ROI, and analyze and characterize their lithological and mineralogical composition. The expected outputs of the trial were maps of the traverse zone and the ROI and a report on the lithology and mineralogy of the rock samples as well as regolith patches in the ROI. The overall size of the mission area was $2500\,\mathrm{m}^2$ and a total time of $2.5\,\mathrm{h}$ was available to solve the challenge. Four operators were allowed in the mission control room. The operators did not have any visibility of the terrain or the robot during the mission. They had to rely on available telemetry and image data to command the robot and take samples.

In this paper, we present team GLIMPSE's approach during the first field trial of the SRC (Fig. 1). As our mobility system, we chose to use a quadrupedal walking robot over a traditional, wheeled or tracked robot. Legged robots such as ANYmal [5] and Spot [6] have advanced rapidly over the last decade and have shown impressive performance in terrestrial environments [7], promising new mobility capabilities in unstructured lunar environments. While general scalability aspects are still a topic of ongoing research [8, 9], several legged prototypes have already been successfully tested on lunar or martian analog terrain [10, 11, 12].

Our solution allowed us to qualify for the SRC's second field trial. This work focuses on our learnings and potential future improvements of the shown system. We are convinced that challenge-driven innovation benefits from participants openly sharing their experiences and lessons learned.

This paper is organized as follows: In Sec. 2, we provide a system overview, including our mobility approach (Sec. 2.1), our localization and mapping framework (Sec. 2.2) and our payload suite (Sec. 2.3). We summarize our field trial outcomes in Sec. 3.1 and give insight into our lessons learned in Sec. 3.2.

2. SYSTEM DESCRIPTION

We use an adapted version of the legged robot ANYmal C by ANYbotics as a mobility platform [13] [5], which we will refer to as ANYmal GLIMPSE in the remainder of this paper. With a mass of $50\,\mathrm{kg}$, a payload capacity of $10\,\mathrm{kg}$, an operation time of $80\,\mathrm{min}$ while continuously walking, ANYmal C is well-suited for the SRC. Using state-of-the-art locomotion control, navigation, and mapping modules, ANYmal C has been successfully used in unknown and rough environments, for example, in the DARPA Subterranean Challenge [14].

ANYmal GLIMPSE is equipped with numerous sensors to localize, navigate, and prospect the environment (Fig. 1). Sensors for localization and navigation include a *VLP16 Puck LITE LiDAR* unit by Velodyne, an *Alphasense Core* visual-inertial sensor by Sevensense Robotics, and two Robosense *RS-BPearl* dome-LiDARs. The VLP16 provides LiDAR scans for LiDAR odometry and mapping. The Alphasense Core, with its three monochrome and four color cameras, as well as four LEDs, provides the operator with a wide field of view to set navigation goals and identify scientific targets. The *RS-BPearls* are mounted at the front and back of the robot and yield the input point clouds for local elevation mapping. Two *Intel Core i7 8850H* and a *Jetson AGX Xavier* graphics processing unit (GPU) provide powerful on-board computing. Rajant's commercial off-the-shelf (COTS) *BreadCrumb DX2* radio ensures network connectivity.

Additionally, ANYmal GLIMPSE is equipped with several scientific payloads, namely a pan-tilt unit with a zoom-camera for close-up and contextual pictures (*CTX*), which is part of the COTS ANYbotics inspection payload, a custom microscope payload (*MICRO*), and a Metrohm *Mira XTR* Raman spectrometer (*RAMAN*). Th scientific payloads are further described in Sec. 2.3.

2.1. Robotic Mobility

Fig 2 shows the main modules in our navigation and locomotion pipeline. The operator can query the map representations built on board via the user interface on mission control, namely the global LiDAR map as a point cloud, the local elevation map, and single LiDAR scans. The operator then provides waypoints sent to the robot via the high-latency network. These waypoints serve as an input to the local planning module [15], which returns a traversable trajectory from the current pose to the target pose using a local elevation map [16]. The path follower module tracks the path and outputs twist commands to the locomotion controller [7].

2.1.1. Locomotion Control

We use a perceptive reinforcement learning-based locomotion controller [7] to achieve robust locomotion in unknown environments. The controller has access to proprioceptive data via the default ANYmal state estimation module based on joint and IMU measurements. Additionally, an elevation mapping module generates a local elevation map based on *BPearl* LiDAR data to provide the controller with exteroceptive information [16]. The controller was trained to balance the proprioceptive and

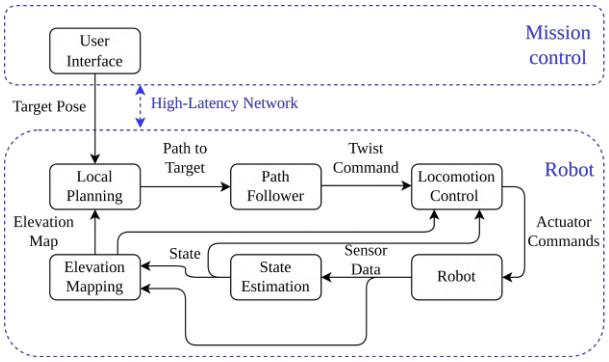

Figure 2: Flowchart of the core modules for robot navigation and locomotion.

exteroceptive information. When the exteroceptive information is reliable, the controller can use it to adapt step height and length proactively and traverse obstacles quickly and smoothly. When the exteroceptive data becomes unreliable due to occlusion, dusty environments, or high-reflectance surfaces, the controller discards it and relies on proprioceptive information. This locomotion controller works reliably on hard-to-traverse terrains such as snow, mud, and rocks. Even in rugged terrain, this controller allows the robot to walk with up to $1.2\,\mathrm{m/s}$. The robustness to noisy and incomplete terrain data makes it highly suitable for unseen and unpredictable environments with adverse lighting conditions in lunar analog missions.

2.1.2. Navigation

As shown in Fig. 2, the user provides local target poses for the robot. We specifically do not use a global planning module because a priori knowledge of the target area is too limited to plan a global traverse to the ROI. On the other hand, the high-latency network does not allow safe and efficient direct teleoperation. We, therefore, deploy the robot in a semi-autonomous fashion: The waypoint provided by the user is fed into a sampling-based local planning module [15] which relies on a local elevation map. Unlike many state-of-the-art navigation planners, this planner does not assign fixed traversability values to discrete terrain patches. Instead, it enforces reachability volumes of the feet to be in contact with the environment while preventing environment collisions of the base for state validity checking. This approach allows to fully utilize the discrete footholds of legged robots, for example, to step over rocks or gaps. The method uses a learned foothold score representation to rate foothold safety and discards surfaces with a low score from the potential foot reachability map. The planning algorithm itself uses a variant of lazyPRM*. The original paper's authors report a maximum planning time of $3.1\,\mathrm{s}$ in their test setup with ANYmal, which allows for real-time use given the robot's speed and the input map size. [15]

The local planner outputs a path from the current robot pose to the target pose. Our path follower module uses a pure-pursuit controller with a look-ahead distance of $1.0\,\mathrm{m}$ to track this path. We limit the forward velocity of the robot in this mode to $0.6\,\mathrm{m/s}$. The twist command generated by the pure pursuit controller serves as an input to the locomotion controller (Sec. 2.1.1).

2.2. Localization and Mapping

The lunar analog conditions, such as high solar incidence angle illumination and granular soil, pose a broad set of challenges to the available localization modules of ANYmal. Leg odometry suffers from severe drift on granular soil, visual-inertial odometry can be inconsistent due to the adverse lighting conditions, and LiDAR odometry is prone to degenerate in structure-less environments.

Consequently, we use a complementary multi-modal localization and mapping approach that relies on a loosely–coupled degeneracy–aware fusion of IMU, leg, and LiDAR odometry [17]. The LiDAR-based odometry and mapping method uses Iterative Closest Point (ICP), which minimizes the distance between two successive point cloud scans. However, optimizing over all points may not lead to an optimal solution. For example, points on a planar surface are not geometrically constrained in their local neighborhood. Prioritizing points that belong to a predefined shape makes the estimation more robust and computationally less expensive. The two most commonly used metrics for point cloud matching are point–to–line distance and point–to–plane distance as used in [18]. Scan-to-map matching can lead to an incorrect robot pose estimate with insufficient geometric constraints. Therefore, the method uses IMU and leg odometry priors to improve the convergence rate of the scan-to-map matching process. Health checks are performed on the LiDAR scan-to-map matching. If LiDAR odometry degenerates, the approach relies on IMU and leg odometry pose estimates to integrate the current point cloud scan into the map. Moreover, IMU and leg odometry provide an update rate of about $200\,\mathrm{Hz}$. Consequently, we use these estimates to propagate the robot pose between LiDAR odometry updates that only occur at $5\,\mathrm{Hz}$.

2.2.1. Global Terrain Mapping

An accurate global terrain map is required to provide an overview of the inspected area. Furthermore, it provides the operator with valuable information for selecting appropriate scientific targets in the ROI. To provide a more expressive representation than raw point clouds, we convert the map from the LiDAR odometry and mapping framework (Sec. 2.2) into a 2.5D model using the grip map library [19]. The point cloud generated by the LiDAR odometry and mapping algorithm stores points that are useful for localization in a volumetric map with a resolution of $20\,\mathrm{cm}$. Since this map may not be dense enough to provide a global 2.5D representation, empty cells are inpainted by filling them with neighboring values. Furthermore, the grid map module discards points higher than $4\,\mathrm{m}$ above the robot.

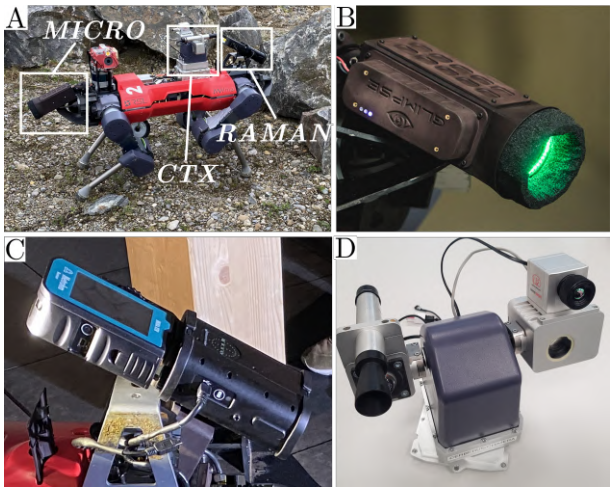

Figure 3: (A) ANYmal GLIMPSE with the three scientific payloads *MICRO*, *RAMAN*, and *CTX*. (B) Close-up MICRO with the visible LED ring. The hull contains the microscope, focus actuation and the control electronics. (C) Close up of RAMAN including the autofocus in black (D) Close-up of the COTS inspection payload by ANYbotics containing CTX, the pan-tilt context imager.

Fig. 5 shows the terrain surface map generated during the first round at the SRC.

2.3. Science Payloads

We rely on a broad scientific payload suite for resource prospection and characterization (Fig. 3). The payloads combine the petrographic and spectrographic analysis of the samples using optical, non-destructive means. The GLIMPSE payload suite consists of three partially complementary instruments:

1. *CTX*: A VIS context imager to obtain high-resolution images of the regolith and the rocks, their size, color, and texture
2. *MICRO*: A multi-wavelength UV-VIS-NIR microscopic imager to get a petrographic image of the samples, their mineral size, assemblages, and distribution, as well as identification of the accessory minerals
3. *RAMAN*: A Raman spectrometer to assess the main mineralogy of the samples.

2.3.1. CTX

CTX is a pan-tilt VIS Context Imager with a resolution of $2.4\,\mathrm{MP}$ and a spectral range of $400\,\mathrm{nm}$ to $950\,\mathrm{nm}$. *CTX* is part of the COTS inspection payload provided by ANYbotics. We use *CTX* to acquire high-resolution RGB context images of selected samples and their environment. *CTX* can acquire images using two different imaging modes:

1. Regular: context image with a fixed horizontal image footprint width of $2.5\,\mathrm{m}$
2. Zoom: close-up image with a fixed horizontal image footprint width of $0.3\,\mathrm{m}$

CTX allows for the morphologic, lithologic, and petrographic description of the samples under varying illumination conditions, namely both from the sunlit and the shadowed side. We further use *CTX* data to characterize the physical properties of the surface material in the ROI and prioritize and contextualize the samples to be studied with the RAMAN payload. To query *CTX* images of a sample, the operator can set a target marker in the onboard computed map at the respective position via the user interface and request a regular or a zoom image. Examples of *CTX* data and results are presented in Fig. 6.

2.3.2. MICRO

MICRO, the UV-VIS-NIR microscopic imager, comprises a Dino-Lite USB microscope (model AD4113T-I2V) integrated into a custom-designed housing, including a linear actuator mechanism and control electronics to focus on the sample surface. Similar microscopic imagers already flew on missions to Mars (Mars Exploration Rovers (MI) [20], MSL Curiosity (MAHLI)[21]) and are also anticipated to fly on the European ExoMars mission (MicrOmega [22], CLUPI [23]).

The microscope has four UV light-emitting diodes (LED) with a peak emittance at $395\,\mathrm{nm}$, and four IR LEDs at $940\,\mathrm{nm}$. The instrument chassis hosts a printed circuit board with 48 additional RGB LEDs (red, green, and blue at $620\,\mathrm{nm}$, $525\,\mathrm{nm}$, and $470\,\mathrm{nm}$, respectively) to cover the entire visible spectrum and illuminate the lunar analog samples independent of the ambient lighting conditions. The LEDs can individually be switched on and off to visually assess the spectral reflectivity at the various wavelengths from UV to NIR. The LEDs are placed in a ring around the microscope. The LED ring enables circular, uniform illumination and illumination from different sides to cast shadows from any specific angle. This approach supports the petrographic assessment of rock samples based on topology and roughness, micro-scale grain size distribution, and mineralogical composition.

The camera's 1.3 megapixel CMOS chip records spectral maps ranging from $390\,\mathrm{nm}$ to $1050\,\mathrm{nm}$. With a working distance of up to $51.7\,\mathrm{mm}$, various magnification rates between 20 – 230x, and a maximum field of view of $25.1\,\mathrm{mm}$ x $20.1\,\mathrm{mm}$, the captured images allow for a reliable petrographic identification by a trained geologist. However, they can also be used to train machine learning-driven classification algorithms.

2.3.3. RAMAN

Raman spectroscopy is an optical, non-destructive analytical technique that provides in-depth information about the sample material, including its chemical composition, phase, crystallinity, and molecular interactions. We use the dust and waterproof Metrohm Raman XTR spectrometer with a $785\,\mathrm{nm}$ scanning laser. This device acquires spatially averaged Raman spectra within a spectral range of $400\,\mathrm{cm}^{-1}$ to $2300\,\mathrm{cm}^{-1}$ and at a resolution of $8\,\mathrm{cm}^{-1}$ to $10\,\mathrm{cm}^{-1}$. It can be used either in standard mode or with an XTR procedure, which provides fluorescence suppression. *RAMAN* is equipped with a telescopic lens with auto-focus capabilities, allowing spectral acquisition from a distance of $0.25\,\mathrm{m}$ to $1.5\,\mathrm{m}$. The auto-focus significantly simplifies operations compared to devices that need to be directly in contact with the sample surface for accurate measurements.

We use a dedicated COTS analysis tool from Metrohm to match acquired spectra against the existing Raman libraries containing spectral data on lunar minerals from the PANGAEA database [24] and previous measurements acquired on different minerals with the Mira XTR. The software outputs a compositional analysis of the investigated sample, including the percent weightings of the various minerals composing the sample. An example of a *RAMAN* measurement is show in Fig. 6.

2.4. Networking

Our software stack mainly uses Robot Operation System (ROS) for inter-process communication. However, ROS is not suited for communication over high-latency networks because TCP handshakes are required for the topic subscription even if the message transport itself runs over UDP. Furthermore, ROS service calls require several handshakes for each call. For these reasons, we use the software package *nimbro_network*[1] for communication between ANYmal GLIMPSE and mission control. *nimbro_network* has been used in several missions to ensure communication over unreliable networks [25][26]. Notably, team CERBERUS used it in their winning approach at the DARPA subterranean challenge [14]. Team NimbRo originally developed it for the DLR SpaceBotCUP. Therefore, the software also closely matches the requirements of the SRC. It contains features such as selectable UDP or TCP transport for both topic and service transport, rate-limiting for each topic, and optimal transparent compression.

Only the core data is constantly streamed to mission control to use minimal network bandwidth. This data includes the TF tree to visualize the robot's position in the map and the camera streams of the Alphasense cameras for navigation. Large data packages that require a lot of bandwidth, such as the LiDAR odometry map or the local elevation map, are only sent on operator request. While constantly streamed data is transferred via UDP, the on-request topics and science payload results are transmitted via TCP to ensure that the data arrives at Mission Control.

[1] https://github.com/AIS-Bonn/nimbro_network

Table 1: Mission overview of GLIMPSE at the first field trail of the SRC.

Traverse Distance to ROI	$107\,\mathrm{m}$
Total Distance travelled	$167\,\mathrm{m}$
Traverse Time	43 min
Total Mission Time	1 h 37 min
CTX images taken	37
RAMAN spectra	3
MICRO images	0

3. RESULTS AND DISCUSSION

3.1. Mission Results

Tab. 1 shows the mission overview in numbers. ANYmal GLIMPSE crossed the traverse area with a path length of $107\,\mathrm{m}$ in $43\,\mathrm{min}$. The robot was able to traverse all three ramps in the traversal region (Fig. 4). The only difficulty in traversing the area was a conservative threshold on the traversability estimation in the local planning module, which forced the operator to bypass the local planning module to traverse the steepest ramp. While the operating speed of the robot ($0.6\,\mathrm{m/s}$) would have allowed a much faster traverse, the main limitation in operating speed was the network communication and the loss of signal. We elaborate further on these issues in Sec. 3.2. We did not observe any significant issues with sinkage on the loose granular soil in the ROI. The robot was able to locomote robustly within the ROI and reach all commanded target poses for payload operations.

As described in Sec. 2.2.1, we generated the global terrain map by running a grid map module over the LiDAR odometry map. We ran the global terrain mapping pipeline on different underlying LiDAR odometry maps for the traverse region and the ROI, respectively. The reason was that early in the mission, the LiDAR odometry maps sent to mission control contained denser data in the traverse region. We further explain this issue in Sec. 3.2.2.

We gathered data from seven scientific targets in the ROI, containing the six rocks of interest and one granular soil sample. We acquired a total of 37 *CTX* images and three Raman spectra. *CTX* was a powerful tool both to enable the scientific analysis of all samples and to prioritize the samples for further payload deployments. We deployed *RAMAN* on two rock samples. The robot took all measurements from the sunlit side with and without XTR. We did not deploy *MICRO* because positioning it close to a sample was difficult and time-consuming. In most cases, the information delivered by *CTX* and *RAMAN* was enough for a rough estimation of the sample lithology and mineralogical composition. Fig. 6 shows an example of the gathered data.

Figure 4: (A) ANYmal GLIMPSE crossing the steepest obstacle in the traverse area. (B) ANYmal GLIMPSE in the ROI. Despite the high sinkage on the granular soil, locomotion worked robustly.

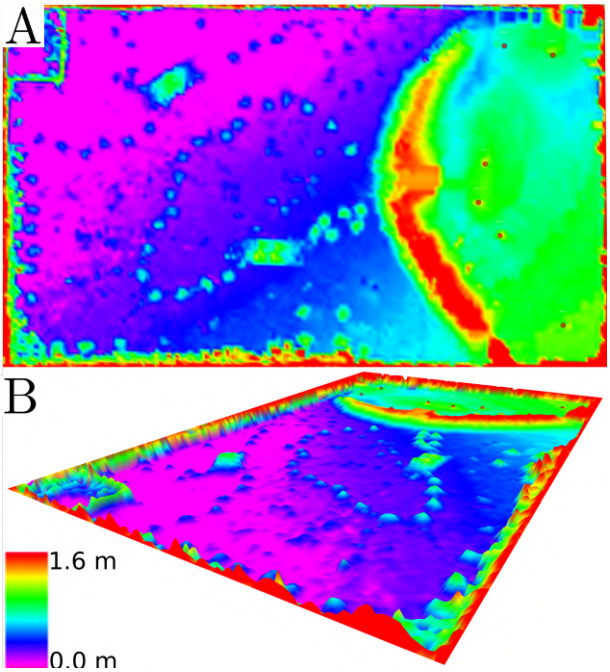

Figure 5: Global terrain maps with indication of the prospected rocks in top (A) and oblique view (B). The colorbar on the bottom left displays the terrain height. Rock positions are indicated with red dots.

3.2. Lessons Learned

3.2.1. Networking

During both our preparation tests and the SRC field trial, we experienced severe networking issues when operating the robot via a delay emulator. Instead of receiving data streams at the nominal frame rate with a 2.5 s delay, data usually arrived tens of seconds late. Data was often entirely lost, for example, when the operator requested *CTX* images. While the robot operation was still possible, a lot of the mission time was lost waiting for data to arrive, for example, to see whether the robot reached the desired target pose. After the SRC field trial, we investigated the network settings more closely. We realized that communication via TCP leads to network congestion because of the excessive time between handshakes. Moving all data transmission to UDP and tuning topic rates mitigated this issue.

3.2.2. Global Terrain Mapping

While the reported global terrain map at the SRC reasonably shows the overall terrain as well as features at around 0.5 m to 1 m, small features are not visible and the overall resolution and accuracy of the map can be drastically improved. One reason for the limited global terrain map quality is that we used the same map for localization and terrain mapping. The LiDAR odometry map used for localization (Sec. 2.2) is down-sampled to reduce the computational burden and be able to run the localization at 5 Hz. However, this down-sampling meant that the grid map module had to work with very few data points of the terrain, which forced us to inpaint the incomplete data and use an early-mission LiDAR odometry map to create the terrain map of the traverse area. In the future, a global terrain mapping approach independent of the localization pipeline could drastically improve the global terrain map because it can be accumulated independent of computational considerations for a localization pipeline. Furthermore, a way of including textures would significantly enhance the usefulness of the global terrain map for future mission planning.

In addition to the global terrain map for scientific operations, a more expressive representation for the robot operator is desirable. During this SRC trial, the operator mainly worked with raw LiDAR scans, local elevation maps, and point clouds from the LiDAR odometry and mapping module. The resolution of this data was often not high enough for a quick assessment of the robot's environment. A dense and expressive operator map representation should contain enough information to make fast decisions during the traverse. However, it still has to be lightweight to prevent network congestion when the operator requests the map.

3.2.3. Autonomy

During our field trials, it became evident that every operator interaction is much more time-consuming over the high-latency network than in terrestrial operations. Every interaction that can be prevented results in a substantial time gain in which the system can collect more

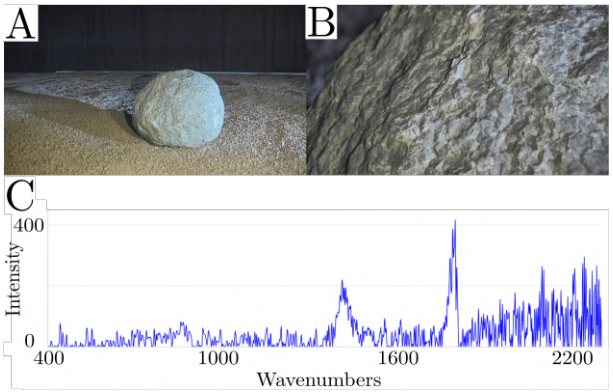

Figure 6: (A) Example of a context image taken with CTX. (B) CTX close-up image. (C) Acquired Raman spectrum of the same rock.

data. While we think that the autonomy we provided during the first SRC trial was a good first baseline, there is still room for substantial improvements. The robot did not have enough autonomy to proceed with the mission for several minutes during a loss of signal, for example, to autonomously continue rock sampling or navigate between samples. During all losses of signal, the robot was standing and waiting for operator commands. Providing this autonomy means that the robot first has to detect the loss of signal and then act according to the current stage of the mission. This decision-making is non-trivial. It depends on how much of the ROI the robot has explored, how many relevant samples it has found, and the data it has collected from these samples. Furthermore, the autonomous operation needs to be very robust to prevent failure cases during a loss of signal. Generally, every autonomy module needs to be highly robust because the operator has no means of quickly aborting dangerous maneuvers via the high-latency network.

3.2.4. Payload Selection and Operation

The *CTX* imager proved to be a powerful tool: On one hand, *CTX* images in regular mode were imperative to localize and prioritize scientific targets for further analysis. On the other hand, zoom images provided an excellent first textural and lithological context of all samples within the ROI, both from the sunlit and shadowed side. However, for a proper mineralogical analysis of the rock samples and regolith, more extensive geochemical mapping with *RAMAN* and *MICRO* is required to support the visual interpretation of the CTX images.

One essential step to achieving more *RAMAN* and *MICRO* samples is the proper placement of these payloads. The rigid mount to the robot's main body made it difficult to properly bring *RAMAN* in position, often requiring several approaches to the sample. For *MICRO*, it was impractical to get the payload close enough to the sample to focus on the sample surface. An additional mechanism is required to position these payloads rapidly and reliably.

3.2.5. Data Processing

In the first field trial, we had no means of assigning data to specific rocks except data time-stamps. This approach is error-prone, and postprocessing the data is inefficient. Furthermore, it does not scale to more data coming in at a higher frequency, for example, when autonomy is improved. Expressive metadata will be critical in the future to enable a fast data evaluation and prevent errors.

4. CONCLUSION

In this work, we presented GLIMPSE, our contribution to ESA SRC's first field trial. We showed that legged locomotion is a powerful solution for rapid and reliable mobility in lunar analog environments when equipped with modern navigation, localization, and locomotion control modules. During the trial, the robot had no issues overcoming the obstacles of the traverse zone or the granular materials in the ROI. GLIMPSE's broad science payload suite allowed for accurate target rocks analysis given the limited mission time.

Based on the lessons learned from this field trial, we consider the following aspects crucial for the next phase of the challenge and potential future mission deployment:

- A high level of autonomy for mobility and data acquisition, especially during loss of signal episodes.
- Accurate global terrain mapping including textural information to understand the geological context of the samples.
- Deployment of all scientific payloads to acquire detailed data to support the visual interpretation of rocks.

We are convinced that these challenges can be overcome and that legged robots will become viable partners for future planetary missions.

ACKNOWLEDGEMENTS

The authors would like to thank the implementation partners, namely the Lucerne University of Applied Sciences and Arts (HSLU), ANYbotics AG, and the maxon SpaceLab. Additionally, the authors would like to thank Metrohm Schweiz AG for providing the Raman spectrometer. We acknowledge the ETH Earth Sciences Collections and University of Basel for their support and for providing rock and mineral samples for our experiments. This work has been conducted as part of ANYmal Research, a community to advance legged robotics.

REFERENCES

[1] ESA, "Esa space resources strategy," 2022.

[2] NASA, "Nasa's plan for sustained lunar exploration and development," 2022.

[3] A. Colaprete, D. Andrews, W. Bluethmann, R. C. Elphic, B. Bussey, J. Trimble, K. Zacny, and J. E. Captain, "An overview of the volatiles investigating polar exploration rover (viper) mission," in *AGU Fall Meeting Abstracts*, vol. 2019, pp. P34B–03, 2019.

[4] S. Li, P. G. Lucey, R. E. Milliken, P. O. Hayne, E. Fisher, J.-P. Williams, D. M. Hurley, and R. C. Elphic, "Direct evidence of surface exposed water ice in the lunar polar regions," *Proceedings of the National Academy of Sciences*, vol. 115, no. 36, pp. 8907–8912, 2018.

[5] M. Hutter, C. Gehring, A. Lauber, F. Gunther, C. D. Bellicoso, V. Tsounis, P. Fankhauser, R. Diethelm, S. Bachmann, M. Blösch, *et al.*, "Anymal-toward legged robots for harsh environments," *Advanced Robotics*, vol. 31, no. 17, pp. 918–931, 2017.

[6] bostondynamics.com, "Boston dynamics," 2022.

[7] T. Miki, J. Lee, J. Hwangbo, L. Wellhausen, V. Koltun, and M. Hutter, "Learning robust perceptive locomotion for quadrupedal robots in the wild," *Science Robotics*, vol. 7, no. 62, p. eabk2822, 2022.

[8] H. Kolvenbach, M. Breitenstein, C. Gehring, and M. Hutter, "Scalability Analysis of Legged Robots for Space Exploration," in *International Astronautical Congress (IAC)*, IAF, Sept. 2017.

[9] H. Kolvenbach, *Quadrupedal Robots for Planetary Exploration*. PhD thesis, ETH Zurich, Institute of Robotics and Intelligent Systems (IRIS), 2021.

[10] H. Kolvenbach, P. Arm, E. Hampp, A. Dietsche, V. Bickel, B. Sun, C. Meyer, and M. Hutter, "Traversing steep and granular martian analog slopes with a dynamic quadrupedal robot," *arXiv preprint arXiv:2106.01974*, 2021.

[11] S. Bartsch, T. Birnschein, M. Römmermann, J. Hilljegerdes, D. Kühn, and F. Kirchner, "Development of the six-legged walking and climbing robot spaceclimber," *Journal of Field Robotics*, vol. 29, no. 3, pp. 506–532, 2012.

[12] A. Rönnau, G. Heppner, M. Nowicki, and R. Dillmann, "Lauron v: A versatile six-legged walking robot with advanced maneuverability," in *2014 IEEE/ASME International Conference on Advanced Intelligent Mechatronics*, pp. 82–87, IEEE, 2014.

[13] "Anybotics ag," 2022.

[14] M. Tranzatto, F. Mascarich, L. Bernreiter, C. Godinho, M. Camurri, S. Khattak, T. Dang, V. Reijgwart, J. Loeje, D. Wisth, *et al.*, "Cerberus: Autonomous legged and aerial robotic exploration in the tunnel and urban circuits of the darpa subterranean challenge," *arXiv preprint arXiv:2201.07067*, 2022.

[15] L. Wellhausen and M. Hutter, "Rough terrain navigation for legged robots using reachability planning and template learning," in *2021 IEEE/RSJ International Conference on Intelligent Robots and Systems (IROS)*, pp. 6914–6921, IEEE, 2021.

[16] T. Miki, L. Wellhausen, R. Grandia, F. Jenelten, T. Homberger, and M. Hutter, "Elevation mapping for locomotion and navigation using gpu," 2022.

[17] S. Khattak, H. Nguyen, F. Mascarich, T. Dang, and K. Alexis, "Complementary multi–modal sensor fusion for resilient robot pose estimation in subterranean environments," in *2020 International Conference on Unmanned Aircraft Systems (ICUAS)*, pp. 1024–1029, IEEE, 2020.

[18] J. Zhang and S. Singh, "Loam: Lidar odometry and mapping in real-time.," in *Robotics: Science and Systems*, vol. 2, pp. 1–9, Berkeley, CA, 2014.

[19] P. Fankhauser and M. Hutter, "A universal grid map library: Implementation and use case for rough terrain navigation," in *Robot Operating System (ROS)*, pp. 99–120, Springer, 2016.

[20] K. E. Herkenhoff, S. Squyres, J. Bell III, J. Maki, H. Arneson, P. Bertelsen, D. Brown, S. Collins, A. Dingizian, S. Elliott, *et al.*, "Athena microscopic imager investigation," *Journal of Geophysical Research: Planets*, vol. 108, no. E12, 2003.

[21] K. S. Edgett, R. A. Yingst, M. A. Ravine, M. A. Caplinger, J. N. Maki, F. T. Ghaemi, J. A. Schaffner, J. F. Bell, L. J. Edwards, K. E. Herkenhoff, *et al.*, "Curiosity's mars hand lens imager (mahli) investigation," *Space science reviews*, vol. 170, no. 1, pp. 259–317, 2012.

[22] J.-P. Bibring, V. Hamm, C. Pilorget, and J. L. Vago, "The micromega investigation onboard exomars," *Astrobiology*, vol. 17, no. 6-7, pp. 621–626, 2017.

[23] J.-L. Josset, F. Westall, B. A. Hofmann, J. Spray, C. Cockell, S. Kempe, A. D. Griffiths, M. C. De Sanctis, L. Colangeli, D. Koschny, *et al.*, "The close-up imager onboard the esa exomars rover: objectives, description, operations, and science validation activities," *Astrobiology*, vol. 17, no. 6-7, pp. 595–611, 2017.

[24] I. Drozdovskiy, G. Ligeza, P. Jahoda, M. Franke, P. Lennert, P. Vodnik, S. J. Payler, M. Kaliwoda, R. Pozzobon, M. Massironi, *et al.*, "The pangaea mineralogical database," *Data in brief*, vol. 31, p. 105985, 2020.

[25] M. Schwarz, T. Rodehutskors, D. Droeschel, M. Beul, M. Schreiber, N. Araslanov, I. Ivanov, C. Lenz, J. Razlaw, S. Schüller, *et al.*, "Nimbro rescue: Solving disaster-response tasks with the mobile manipulation robot momaro," *Journal of Field Robotics*, vol. 34, no. 2, pp. 400–425, 2017.

[26] J. Stückler, M. Schwarz, M. Schadler, A. Topalidou-Kyniazopoulou, and S. Behnke, "Nimbro explorer: Semiautonomous exploration and mobile manipulation in rough terrain," *Journal of Field Robotics*, vol. 33, no. 4, pp. 411–430, 2016.